CHEMISTRY
A EUROPEAN JOURNAL

DOI: 10.1002/chem.201000639

General Strategy for a Large-Scale Fabric with Branched Nanofiber–Nanorod Hierarchical Heterostructure: Controllable Synthesis and Applications

Meng Shang, Wenzhong Wang,* Wenzong Yin, Jia Ren, Songmei Sun, and Ling Zhang[a]

Abstract: The preparation and characterization of a branched nanofiber–nanorod hierarchical heterostructure fabric (TiO_2/NiO, TiO_2/ZnO, and TiO_2/SnO_2) are described. The nanomaterial was synthesized on a large scale by an inexpensive, generalizable, facile, and controllable approach by combining the electrospinning technique with a hydrothermal method. The controllable formation process and factors (assistance by hexamethylenetetramine and metal oxide nuclei) influencing the morphology of the branched hierarchical heterostructure are discussed. In addition, photocurrent and photocatalytic studies suggest that the branched hierarchical heterostructure fabric shows higher mobility of charge carriers and enhanced photocatalytic activity relative to a bare TiO_2 nanofibrous mat and other heterostructures under irradiation by light. This work demonstrates the possibility of growing branched heterostructure fabrics of various uniform, one-dimensional, functional metal oxide nanorods on a TiO_2 nanofibrous mat, which has a tunable morphology by changing the precursor. The study may open a new channel for building hierarchical heterostructure device fabrics with optical and catalytic properties, and allow the realization of a new class of nano-heterostructure devices.

Keywords: heterostructures · nanofibers · nanostructures · structure–activity relationship · synthesis design

Introduction

One-dimensional (1D) functional semiconductor oxides, such as nanowires, nanorods, and nanotubes, have attracted great worldwide interest mainly because of their large aspect ratio, single-crystal properties, and the directional mobility of charge carriers in these systems. 1D semiconductor oxides have also been used as building blocks for a number of nanoscale photonic and electro-optical devices.[1–7] Driven by this, manipulations with a given nanoscale object have not only generated pure nanomaterials with novel properties, but also achieved multicomponent nanosystems (heterostructures) with diverse functions. 1D nanoscale hierarchical heterostructures with modulated morphologies, compositions, and interfaces have obtained considerable attention.[8–11] Especially, new hierarchical heterostructures, in which the major 1D cores and branches consist of different materials, have attracted particular interest.[12,13] So far, there have been a number of reports on branched 1D nanostructures synthesized by two-step or multistep catalyst-assisted metal–organic chemical vapor deposition methods and metal–organic vapor-phase epitaxy methods.[14–18] Demonstrated materials include ZnO, In_2O_3/ZnO, Si, CdS, and ZnS/SiO_2. However, these methods require extreme conditions, special equipment, and the products cannot be mass-produced, which hampers their practical applications. In this case, it would be a viable and complementary advance to develop a facile and practical approach to synthesize 1D branched hierarchical heterostructures. Such an approach could avoid i) the high temperature, ii) the expensive and complicated equipment, and iii) the potential toxic precursors and by-products.

Electrospinning,[19–21] a comparatively low-cost and applicable technique, is able to synthesize materials in the form of fabric with a certain strength and flexibility on a large scale. This nanofibrous fabric could be manipulated more easily than other forms, such as particles, powders, and films. Moreover, the electrospun nanofibers with both high porosity and large surface area are promising materials for surface modification and functionalization. Another chemical technique, the hydrothermal method, has also been proven to be

[a] M. Shang, Prof. W. Wang, W. Yin, J. Ren, S. Sun, Dr. L. Zhang
State Key Laboratory of High Performance Ceramics and Superfine Microstructure
Shanghai Institute of Ceramics, Chinese Academy of Sciences
1295 DingXi Road, Shanghai 200050 (P. R. China)
Fax: (+86) 21-5241-3122
E-mail: wzwang@mail.sic.ac.cn

Supporting information for this article is available on the WWW under http://dx.doi.org/10.1002/chem.201000639.

a powerful procedure owing to its environmentally friendly approach, low temperature, and the controllable morphology obtained. It has been demonstrated that the hierarchical heterostructure can greatly improve its performance by use of the advantages of the electrospinning and hydrothermal methods.[22] Currently, however, the growth of the heterostructure occurs almost naturally on its own crystal habit, and has not yet been controlled uniformly. Much more effort should be employed to further enhance the comprehensive properties of these materials for practical application by tuning the shape and size of the 1D hierarchical heterostructure. Furthermore, the general large-scale synthesis of different metal oxides (MOs) with a branched hierarchical heterostructure remains a tremendous challenge, because it is very difficult to control the growth of different MOs into branched nanostructures on the surface of nanofibers uniformly and densely. Thus, it is highly appealing to establish a general method that uses safe, inexpensive, and "user-friendly" reagents to synthesize various branched hierarchical heterostructures with different functionalities. This would open up possibilities for the extensive study of the physical and chemical properties of the most promising nanostructures and extend their practical applications.

Motivated by the above concerns, in this work we developed a general approach for the large-scale synthesis of a series of uniform 1D functional MOs, such as NiO, ZnO, and SnO_2, on TiO_2 nanofibrous mats to form a branched nanofiber–nanorod hierarchical heterostructure (TiO_2/MO) by combining the electrospinning technique with the hydrothermal method. Compared with the previous strategy, this approach is reproducible and enables excellent control over the hetero-nanoarchitectures. The morphology of the nanostructured MO can be varied easily by simply tuning the precursor. The as-prepared fabric obtained by this general approach has shown higher mobility of charge carriers and enhanced photocatalytic activity, which exemplifies the excellent properties of such branched hierarchical heterostructures. Moreover, these hierarchical heterostructure fabrics are structurally well defined and can be generated in reasonable quantities, which could be the framework for devices and systems in practical applications. The key point is that our method is generalizable and can be adapted to the production of families of branched hierarchical heterostructures (TiO_2/MO), which are the focus of our efforts herein.

Results and Discussion

The overall synthesis procedure employed for the preparation of branched TiO_2/MO hierarchical heterostructures is illustrated in Figure 1, and is briefly composed of two steps. First, a TiO_2 nanofibrous mat was electrospun from a Ti-$(OBu)_4$ sol at an appropriate voltage, and then the obtained nonwoven film was calcined to form an anatase and rutile TiO_2 nanofibrous mat. Second, the electrospun TiO_2 nanofibrous mat was placed into an autoclave containing an MO sol and metal salt (M^{n+})–hexamethylenetetramine (HMT)–

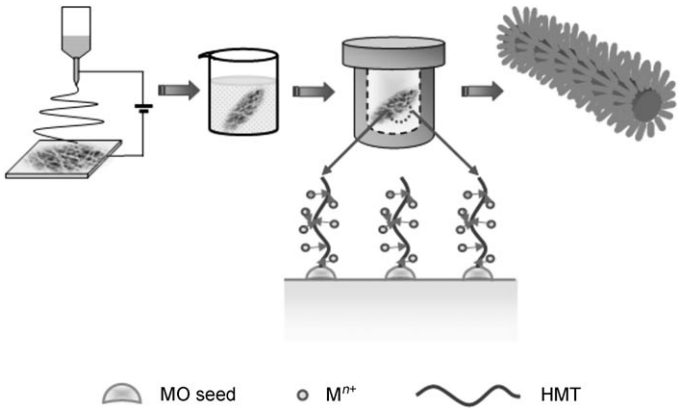

Figure 1. Preparation of the branched TiO_2/MO hierarchical heterostructure fabric.

H_2O solution. The hydrothermal reaction process was carried out at a desired temperature and time. As a result, perfectly branched TiO_2/MO hierarchical heterostructure fabrics were obtained in high yield. The detailed mechanism for forming this morphology by the general approach will be illustrated later.

Preparation of a branched TiO_2/NiO hierarchical heterostructure: The synthesis of the branched TiO_2/NiO hierarchical heterostructure was performed first to show that the TiO_2 nanofibrous mat was covered with a dense layer of NiO nanorods forming a branched morphology by using a controllable hydrothermal method at 180 °C for 20 h.

A typical scanning electron microscopy (SEM) image of such a structure is shown in Figure 2A. In general, the TiO_2 nanofibrous backbones can be as long as tens of micrometers with a relatively smooth surface by using the electrospinning method, and could be fabricated on a large scale according to practical requirements (see Supporting Information, Figure S1). This is one of the advantages of the electrospinning method.[22d] After applying the controllable solution growth of NiO nanorods, the hierarchical heterostructure resembled the leaves of a pine tree (Figure 2A). The diameter of the hierarchical nanofibers was about 600 nm. Close observation of the nanofibers (Figure 2B) reveals that a high density of secondary NiO nanorods was uniformly dispersed on the primary TiO_2 substrate. The nanorod branches stand nearly perpendicular to the surface of the TiO_2 nanofibers. The high-magnification SEM image of a single nanofiber (Figure 2C) further shows that the length of the secondary NiO nanorods grown on the TiO_2 backbone ranges from 200 to 400 nm with a diameter of about 80 nm. In addition, many pores with different diameters, which may serve as transport paths for small molecules and utilize light efficiently, are found among the nanorods and nanofibers in this hierarchical heterostructure.

The structure was further examined by transmission electron microscopy (TEM). The TEM image in Figure 2D shows an individual TiO_2/NiO hierarchical nanofiber. It was confirmed that the whole diameter of the hierarchical nano-

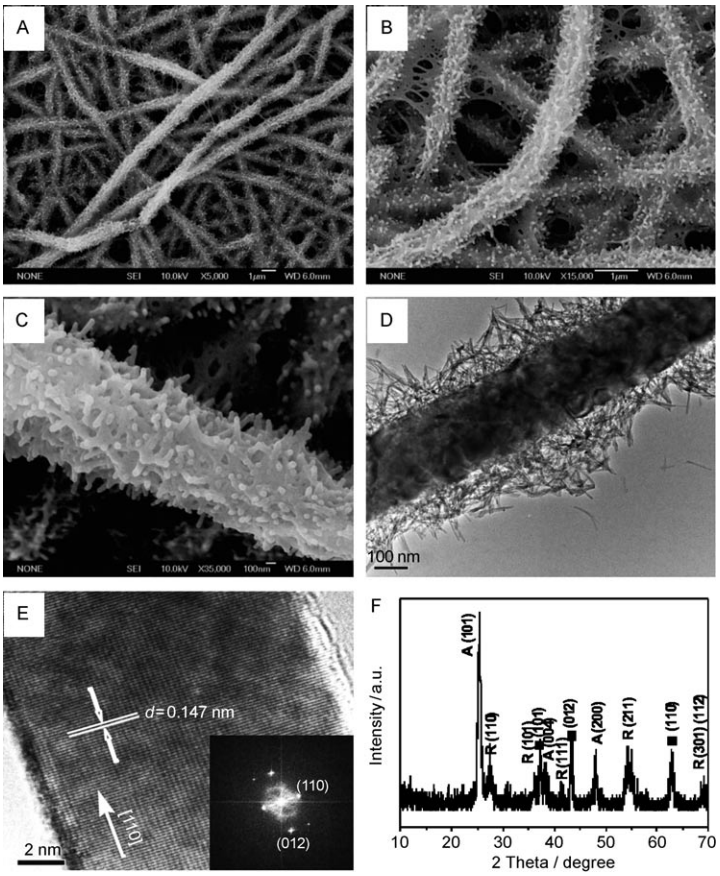

Figure 2. A) SEM image of the overall morphology of the branched TiO_2/NiO hierarchical heterostructure fabric. B) Detailed view of branched TiO_2/NiO hierarchical nanofibers. C) A single nanofiber. D) TEM image of an individual TiO_2/NiO hierarchical nanofiber. E) HRTEM image of a NiO nanorod. Inset: 2D FFT of the lattice image. F) XRD pattern of the TiO_2/NiO hierarchical heterostructure. ■ indicates the rhombohedral NiO; A: anatase; R: rutile.

fibers was about 600 nm, which agrees well with that revealed by the SEM images. Each NiO nanorod is of uniform diameter along its entire length. Now we come closer to the NiO nanorods, from which the high-resolution TEM (HRTEM) image and the 2D fast Fourier transform (FFT) of the lattice image of the NiO nanorod were recorded (Figure 2E). The NiO branch is single-crystalline with clear lattice fringes. The interlayer distance is consistent with the interplanar distance of the (110) plane of NiO (0.147 nm). This means that the NiO nanorod is single-crystalline and the growth is along the [110] direction. It has been demonstrated that the single-crystalline material with 1D nanostructure has the property of fast directional migration of charge. Therefore, this branched heterostructure is assumed to exhibit higher mobility of charge carriers and enhanced photocatalytic activity.

Subsequently, X-ray diffraction (XRD) analysis was performed to investigate the crystal phase of the TiO_2/NiO hierarchical heterostructure (Figure 2F). The typical XRD pattern indicates that all the diffraction peaks of the TiO_2/NiO heterostructures can be well indexed as the anatase TiO_2 (JCPDS No. 73-1764), rutile TiO_2 (JCPDS No. 21-1276), and rhombohedral NiO (JCPDS No. 44-1159) phases. No other impurity peaks are detected, which indicates the absence of other impurities. Besides, no remarkable shift in diffraction peak was detected, which indicates that no obvious interface reaction between TiO_2 and NiO occurred. It is obvious that the synthesis route adopted successfully achieves a TiO_2/NiO heterostructure integrating the rhombohedral NiO and the TiO_2 anatase and rutile phases.

Preparation of branched TiO_2/ZnO and TiO_2/SnO_2 hierarchical heterostructures: This approach can be easily extended to the synthesis of other 1D functional oxides with heterostructures in high yield. In the case of ZnO, a relatively low temperature (100 °C for 3 h) was used to fabricate the branched TiO_2/ZnO hierarchical heterostructure. The low-magnification SEM image (Figure 3A) shows the relatively uniform secondary ZnO nanorods grown on the primary TiO_2 substrates. It can be seen from the high-magnification SEM image (Figure 3B) that the hydrothermally generated ZnO nanorods are of lengths ranging from 200 to 400 nm and diameters of about 100 nm. Furthermore, it has been identified that the nanorods have a hexagonal end face, which is the typical crystal habit and growth form of ZnO (wurtzite structure).[23] The XRD pattern also confirmed that all diffraction peaks can be indexed as the anatase TiO_2 (JCPDS No. 73-1764), rutile TiO_2 (JCPDS No. 21-1276), and hexagonal ZnO (JCPDS 36-1451) phases (see Supporting Information, Figure S2). The structure was further examined by TEM (see Figure 3C); the image of an individual ZnO nanorod shows that the nanorod is of uniform diameter (about 100 nm) along its entire length. This indicates that

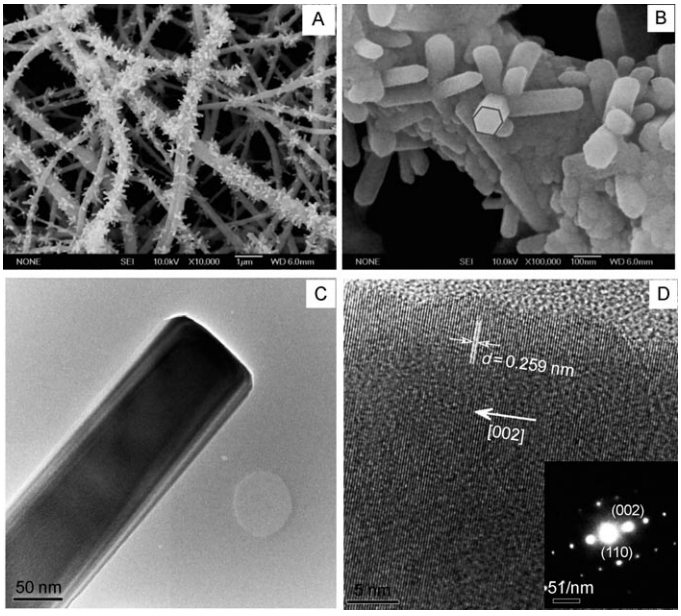

Figure 3. A) SEM image of the overall morphology of the branched TiO_2/ZnO hierarchical heterostructure fabric. B) A single nanofiber. C) TEM image of an individual TiO_2/ZnO hierarchical nanofiber. D) HRTEM image of a ZnO nanorod. Inset: ED pattern.

the growth anisotropy is strictly maintained in the *c* axis throughout the whole growth stage. Moreover, the contrast between the dark center and the pale edge provides convincing evidence of the hexagonal structure. The HRTEM image (Figure 3D) further confirms the single-crystalline structure of the ZnO nanorods with a lattice spacing of 0.259 nm from the (002) face. The electron diffraction (ED) pattern of an individual ZnO nanorod grown on a TiO_2 nanofiber can be indexed as [$\bar{1}$10] zone spots (inset in Figure 3D). These mean that the ZnO nanorod is single-crystalline and that growth is along the [002] direction.

Similarly, the branched TiO_2/SnO_2 hierarchical heterostructure can also be easily synthesized through this general approach. As shown in Figure 4A, the diameter of the TiO_2/

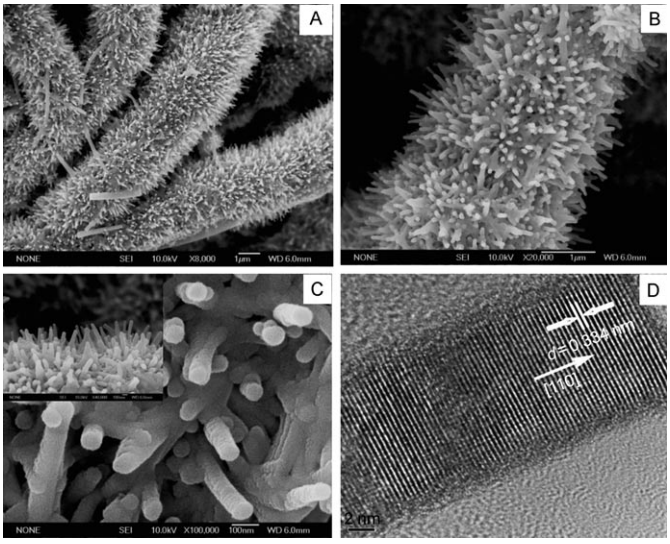

Figure 4. A) SEM image of the overall morphology of the branched TiO_2/SnO_2 hierarchical heterostructure fabric. B) A single nanofiber. C) TEM image of the individual TiO_2/SnO_2 hierarchical nanofiber. D) HRTEM image of an SnO_2 nanorod.

SnO_2 hierarchical nanofibers was up to about 3 μm by using the controllable solution growth of uniform and dense SnO_2 nanorods on the surface of TiO_2 nanofibers. Upon magnifying a single nanofiber (Figure 4B), it can be seen that the morphology of this branched TiO_2/SnO_2 hierarchical heterostructure was similar to that of the TiO_2/NiO product except for the longer length of the SnO_2 nanorods, which was about 1 μm. The high-magnification SEM image from the top of the SnO_2 nanorods shows that the diameter of the secondary nanorods is about 80 nm (Figure 4C), and nearly every SnO_2 nanorod branch was oriented in a perpendicular fashion to the surface of the TiO_2 nanofibers (see the inset of Figure 4C). The HRTEM image (Figure 4D) further confirms the single-crystal structure of the SnO_2 nanorods with a lattice spacing of 0.334 nm on the (110) face. Furthermore, the XRD pattern confirmed that all diffraction peaks can be indexed to the anatase TiO_2 (JCPDS No. 73-1764), rutile TiO_2 (JCPDS No. 21-1276), and tetragonal SnO_2 (JCPDS 41-1445) phases (see Supporting Information, Figure S3). This means that the SnO_2 nanorod is single-crystalline and the growth is along the [110] direction.

Formation mechanism of the branched hierarchical heterostructure: To sum up, it has been demonstrated that a series of branched TiO_2/MO hierarchical heterostructures have been synthesized in a general and facile way by combining the electrospinning technique with the controllable hydrothermal method. The controllable formation process of the branched heterostructure is schematically illustrated in Figure 1.

Before the hydrothermal process, the pristine TiO_2 nanofibrous mat has to attach a layer of MO seed nanoparticles by dip-coating as specific nucleation sites. It is noted that the seed layer is mandatory because no secondary growth to form a branched morphology was observed when this step was omitted. Taking NiO as an example, as shown in Figure 5, only the longer nanorods dispersed on the TiO_2

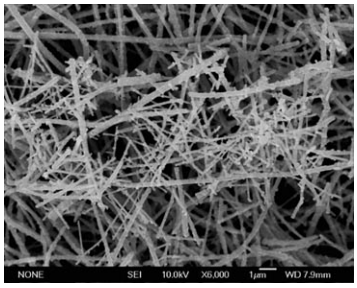

Figure 5. SEM image of the TiO_2/NiO sample prepared without NiO seeds under hydrothermal conditions.

nanofibers and no branched TiO_2/NiO hierarchical heterostructures were obtained. In this key step, the uniform small nuclei play an important role in determining the growth kinetics of small nanorods on the surface of TiO_2 nanofibers. Firstly, the uniformity of nanoparticles obtained by the sol method is very important for a narrow size distribution of nanorods. In the current hydrothermal process to obtain the nanorod arrays, MO seeds synthesized by the sol method are deposited on the TiO_2 substrates. The crystal growth kinetics process is the epitaxial heterogeneous nucleation on the existing nuclei when nanorods grow from the nucleation sites of the seed layer. However, the homogeneous nucleation occurs in the supersaturated aqueous solution if there is no crystal seed limitation. As a result, the nanorods grow at a fast rate and tend to form a longer length under hydrothermal conditions (Figure 5). Secondly, the lattice matching between MO nanorods and the nucleus seeds (MO nanoparticles) is crucial to the crystal growth on the seed surface. They have the same crystal type, and provide the best matching and lowest energy barrier to obtain the branched heterostructure.

The general chemical reactions in the following hydrothermal deposition process involving HMT and a desired

metal salt as reactants can be expressed as follows [Eqs. (1)–(3)]:[23–25]

$$(CH_2)_6N_4 + 6H_2O \xrightarrow{\Delta} 6HCHO + 4NH_3 \quad (1)$$

$$NH_3 + H_2O \rightarrow NH_4^+ + OH^- \quad (2)$$

$$nOH^- + M^{n+} \rightarrow M(OH)_n \rightarrow MO_{(s)} + \frac{n}{2}H_2O \quad (3)$$

The initial pH of the metal salt and HMT solution is 6.7 and remains relatively constant throughout the nucleation and growth processes. For this pH and the metal salt concentration used (0.05 M), the predicted dominant metal species present will be hydrated M^{n+}. With prolonged heating, the solution will contain partially decomposed HMT complexes, ammonia (NH_3), and formaldehyde (HCHO) with the vapor containing a mixture of H_2O, NH_3, and HCHO.[26] Due to the decomposition of metal salt and HMT at elevated temperature, the concentration of M^{n+} and OH^- increases correspondingly. Finally, $M(OH)_n$ or MO nuclei start to form when the degree of supersaturation surpasses a critical value. In the whole process, the precursors are consumed for the growth of MO on the nuclei seeds, and the precursor concentration decreases quickly. Therefore, it was assumed that the branched TiO_2/MO hierarchical heterostructures were hardly obtained under the conditions of a lower metal salt concentration. Figure 6 shows representative SEM images of hierarchical TiO_2/NiO nanostructures obtained by decreasing the concentration of metal salt and HMT (0.01 M), while keeping their 1:1 ratio unchanged. Obviously, both the density and diameter of the secondary NiO nanorods decrease directly with the concentration of salts. The high-magnification SEM image shows that the diameter of the secondary nanorods is less than 100 nm (Figure 6B), which is similar to the nanoparticles on the surface of the TiO_2 nanofibers.

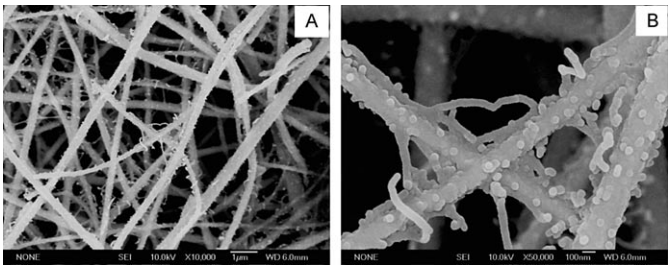

Figure 6. SEM images of hierarchical TiO_2/NiO nanostructures prepared by decreasing the concentration of metal salt and HMT (0.01 M). A) Lower-magnification SEM image. B) Higher-magnification SEM image.

It is noticeable that the HMT was crucial in the formation of the MO nanorods. The branched products could only be obtained in the presence of an appropriate amount of HMT. A different agent, NaOH instead of HMT, was applied in the reaction system in our experiment. No branched structures were observed. The morphology of the secondary MO nanostructures is tailored to another nanostructure by changing the HMT to NaOH during the hydrothermal process. Figure 7 shows the TiO_2/NiO hierarchical heterostructure using NaOH as the source of OH^-. Instead of a 1D branched nanostructure, 2D layers of NiO nanosheets on the TiO_2 nanofibers (TiO_2/NiO nanosheets) were obtained. The NiO nanosheets are about 100 nm in thickness and about 1 μm in length (Figure 7B). It is demonstrated that the slow degradation of HMT at elevated temperature and the rise of pH value (buffer effect) are important factors that contribute to anisotropic growth and result in perspective and an interesting 1D morphology of MO nanostructures.[23,27,28]

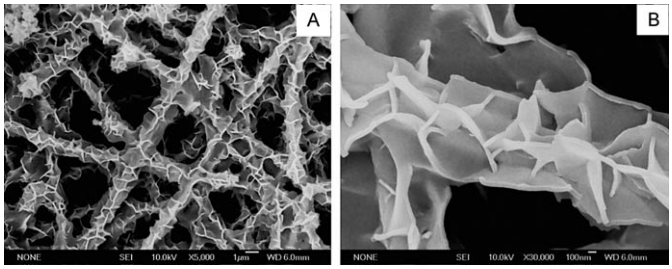

Figure 7. SEM images of the TiO_2/NiO hierarchical heterostructure using NaOH as the source of OH^-. A) Lower-magnification SEM image. B) Higher-magnification SEM image.

Photocurrent investigation: The mobility capability of electrons generated in the semiconductors under light irradiation can be directly monitored by the photocurrent.[29] Figure 8 shows the photocurrent density of the samples generated in suspensions under UV–visible light. It is noted that the photocurrent density of the branched TiO_2/NiO hierarchical heterostructure is approximately 1.5 times higher than that of the TiO_2 nanofibrous mat. This indicates that carriers transfer faster to the surface of the TiO_2/NiO heterostructure than they do in the TiO_2 nanofibrous mat. There-

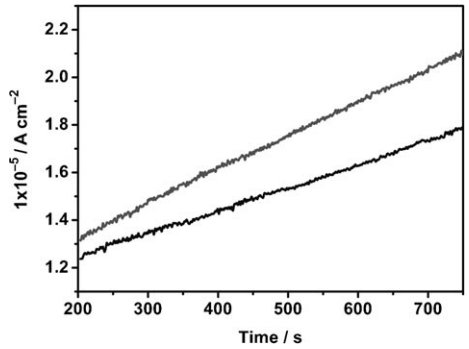

Figure 8. Photocurrent density as a function of light irradiation time over TiO_2/NiO (gray line) and TiO_2 (black line) samples.

fore, it can be concluded that the branched hierarchical heterostructure promotes the transfer rate of carriers to the sample surface. Overall, our results intimate that the as-prepared samples have high mobility of charge carriers and high-quality optical properties, which may lead to several practical applications.

Photocatalytic activity: The applications in solar-energy conversion and degradation of pollution by semiconductor photocatalysts have received extensive attention in modern society. It has been proven that the photocatalytic activity is also closely related to the structure and the efficiency of the photogenerated electron–hole diffusion from the inner regions to the surface.[30] The photocatalytic degradation of aqueous ammonia, a major nitrogen-containing pollutant, was performed at pH 10.8.[31] As shown in Figure 9, under

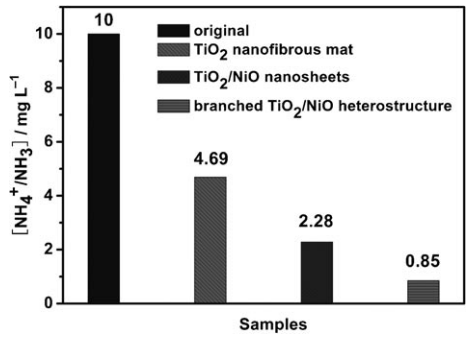

Figure 9. Photocatalytic degradation of NH_4^+/NH_3 in the presence of as-synthesized photocatalysts.

light irradiation for 3 h the concentration of NH_4^+/NH_3 decreases from an initial $10\,mg\,L^{-1}$ to approximately $0.85\,mg\,L^{-1}$ in the presence of the branched TiO_2/NiO hierarchical heterostructure fabric, and more than 90% of NH_4^+/NH_3 was degraded. Only 53 and 77% of the NH_4^+/NH_3 were degraded after 3 h in the presence of the TiO_2 nanofibrous mat and TiO_2/NiO nanosheets, respectively, thus indicating the excellent photocatalytic performance of the branched TiO_2/NiO hierarchical heterostructure fabric. Furthermore, the separability and the stability of the high photocatalytic performance of the as-prepared sample were also confirmed by circulating runs in the photocatalytic degradation of aqueous ammonia (see Supporting Information, Figure S4). The branched TiO_2/NiO hierarchical heterostructure fabric could be easily recycled without deactivation, which indicated that the large-scale fabric did not photocorrode during the photocatalytic oxidation of the pollutant molecules, which is especially important for its application.

The potential photocatalytic mechanism in the degradation of pollutant has been previously described and may involve several steps: 1) photoabsorption of the TiO_2/MO catalysts, 2) generation of photoinduced electrons and holes, and 3) transfer of charge carriers to the surface.[32,33] The photocatalysis proved that the branched TiO_2/MO hierarchical heterostructure fabric prepared by the facile and general method presents enhanced photocatalytic activity, which is most likely affected by many correlated factors. The Brunauer–Emmett–Teller (BET) surface area of the branched TiO_2/NiO hierarchical heterostructure fabric was estimated to be about $36.68\,m^2\,g^{-1}$, which was much higher than that of the TiO_2 nanofibrous mat ($6.92\,m^2\,g^{-1}$) or TiO_2/NiO nanosheet sample ($15.1\,m^2\,g^{-1}$). The high surface area and plenty of pores in the 3D branched hierarchical heterostructure allow not only more surface to be reached by the incident light but also more active catalytic sites, which results in good photocatalytic performance.[34] Moreover, the TiO_2/MO samples prepared by combining the electrospinning technique with the hydrothermal method provide a heterogeneous structure. On the basis of the relative energy level of TiO_2 and MO, the photogenerated holes and the photogenerated electrons can be promoted by the internal field, which results in charge separation and stabilization, thus hindering the recombination process. The photocurrent investigation (Figure 8) can also prove that the heterostructure could promote the transfer rate of carriers to the sample surface. A larger number of electrons and holes on the catalyst surface can participate in photocatalytic reactions to directly or indirectly mineralize organic pollution, and thus the photocatalytic reaction can be enhanced greatly (see Supporting Information, Figure S5). Besides, the higher photocatalytic activity of the branched TiO_2/MO hierarchical heterostructure fabric can also be ascribed to the branched nanostructure. It has been reported that high-quality 1D nanostructured semiconductors have been considered as model systems for efficient transport of electrons and optical excitations.[5,35] As a result, the branched TiO_2/NiO hierarchical heterostructure fabric showed higher photocatalytic activity than the TiO_2/NiO nanosheet sample (Figure 9). More importantly, as schematically illustrated in Figure 10, we believe that the unique branched hierarchical

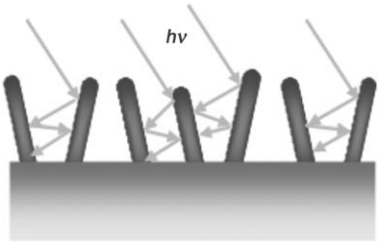

Figure 10. Schematic illustration of multireflections within the branched hierarchical heterostructure.

heterostructure with an appropriate space between the nanorods allows multiple reflections of electromagnetic waves, such as ultraviolet and visible light,[36] thus allowing more efficient use of the light source and therefore endowing these branched hierarchical heterostructure fabrics with greatly enhanced properties.

Conclusion

A family of branched nanofiber–nanorod hierarchical heterostructure fabrics including TiO_2/NiO, TiO_2/ZnO, and TiO_2/SnO_2 has been successfully synthesized on a large scale by a facile and general approach by combining the practical electrospinning technique with the controllable hydrothermal method. The number density and morphology of the secondary 1D MO nanostructure can be tuned by simply adjusting the precursor conditions, which is also the key point to obtaining the branched morphology. The as-prepared branched TiO_2/MO fabric exhibited higher mobility of charge carriers and practically enhanced the photocatalytic activity, which is correlated with the hierarchical heterostructure and spatial 3D arrangement of the 1D nanorods. Moreover, the present general method is quite simple, environmentally benign, and cost-effective, thus permitting it to be developed for the design of other complex heterostructured fabric systems that might find potential applications in many fields, such as catalysis, chemical/biological separation, sensing, lasers, and solar-energy conversion devices.

Experimental Section

Materials: Poly(vinyl pyrrolidone) (PVP) with a molecular weight (MW) of 1.3×10^6 was obtained from Aldrich; other reagents were of analytical purity and were used as received from Shanghai Chemical Company. The TiO_2 nanofibrous mat was prepared according to the previous study.[22d]

Synthesis of branched TiO_2/MO hierarchical heterostructure fabric: Typically, the desired metal salt ($NiCl_2$, $Zn(NO_3)_2$, $SnCl_4$) was dissolved in ethanol (100 mL) and the solution was heated at 80 °C for 2 h. Tetramethylammonium hydroxide (TMAH) was added to adjust the pH value of the final suspension to about 10. Then the mixture was stirred for 1 h at room temperature. Afterwards, the mixture was exposed to high-intensity ultrasonic irradiation (6 mm diameter Ti-horn, 300 W, 20 kHz) at room temperature in ambient air for 30 min and an MO sol was obtained. Subsequently, the TiO_2 (1.2 mmol) nanofibrous mat was immersed in the as-prepared MO sol for 10 min to coat it with MO nanoparticles as seeds, and then, with MO sol (10 mL), it was immediately put into an autoclave containing an aqueous solution (30 mL) of equimolar amounts of metal salt and HMT (forming a 0.05 M solution). Then the autoclave was sealed and heated at 180 °C for 20 h (NiO), at 100 °C for 3 h (ZnO), or at 180 °C for 12 h (SnO_2). The fabric was washed with deionized water and ethanol to remove any ionic residual material and then dried in an oven at 80 °C for 4 h.

Characterization: The XRD patterns of the samples were measured on a D/MAX 2250 V diffractometer (Rigaku, Japan), with monochromated $Cu_{K\alpha}$ ($\lambda=0.15418$ nm) radiation at 40 kV and 100 mA and scanning over the range of $10°\le2\theta\le70°$. The morphologies and microstructures of the as-prepared samples were analyzed by SEM (JEOL JSM-6700F) and TEM (JEOL JEM-2100F, accelerating voltage 200 kV). Nitrogen adsorption–desorption measurements were conducted at 77.35 K on a Micromeritics Tristar 3000 analyzer after the samples were degassed at 200 °C for 6 h. The BET surface areas of the products were estimated by using the adsorption data.

Photocurrent measurement: Photocurrent measurements were performed by using a CHI 660C electrochemical workstation. A photocatalyst (25 mg) was suspended in deionized H_2O (75 mL) containing acetate (0.1 M) and Fe^{3+} (0.1 mM) as an electron donor and acceptor, respectively. A Pt plate (1×1 cm^2, 0.125 mm thick, both sides exposed to solution), a saturated calomel electrode (SCE), and a Pt gauze were immersed in the reactor as working (collector), reference, and counter electrodes, respectively. Photocurrents were measured by applying a potential (+1 V vs. SCE) to the Pt electrode with a potentiostat (EG&G). All experiments were conducted at about 25 °C.

Photocatalytic experiments: Photocatalytic activities of the as-prepared samples were evaluated by the degradation of aqueous ammonia under UV–visible light irradiation with a 500 W Xe lamp. The photocatalyst (0.1 g) was added to NH_4Cl solution (100 mL), the pH value of which was adjusted to 10.8 by aqueous NaOH. Before illumination, the solution was stirred for 120 min in the dark to reach the adsorption–desorption equilibrium between the photocatalyst and NH_4^+/NH_3. The concentration of NH_4^+/NH_3 was estimated before and after the treatment using the Nesster's reagent colorimetric method.

Acknowledgements

This work was supported by the National Natural Science Foundation of China (No. 50972155), National Basic Research Program of China (973 Program, 2007CB613302), and the Nanotechnology Programs of the Science and Technology Commission of Shanghai (0852nm00500, 0952nm00400).

[1] a) Y. Cui, Q. Q. Wei, H. K. Park, C. M. Lieber, *Science* **2001**, *293*, 1289; b) M. H. Huang, S. Mao, H. Feick, H. Yan, Y. Wu, H. Kind, E. Weber, R. Russo, P. Yang, *Science* **2001**, *292*, 1897; c) F. Favier, E. C. Walter, M. P. Zach, T. Benter, R. M. Penner, *Science* **2001**, *293*, 2227.

[2] a) R. E. Presley, C. M. Munsee, C. H. Park, D. Hong, J. F. Wagner, D. F. Keszler, *J. Phys. D* **2004**, *37*, 2810; b) B. G. Lewis, D. C. Paine, *MRS Bull.* **2000**, *25*, 22.

[3] a) Z. R. R. Tian, J. A. Voigt, J. Liu, B. McKenzie, M. J. McDermott, M. A. Rodriguez, H. Konishi, H. F. Xu, *Nat. Mater.* **2003**, *2*, 821; b) J. H. Woodruff, J. B. Ratchford, I. A. Goldthorpe, B. C. McIntire, C. E. D. Chidsey, *Nano Lett.* **2007**, *7*, 1637.

[4] a) Y. J. Chen, C. L. Zhu, T. H. Wang, *Nanotechnology* **2006**, *17*, 3012; b) F. Hernandez-Ramirez, A. Taracon, O. Casals, E. Pellicier, J. Rodriguez, A. Romano-Rodriguez, J. R. Morante, S. Barth, S. Mathur, *Phys. Rev. B* **2007**, *76*, 085429; c) F. Hernandez-Ramirez, S. Barth, A. Taracon, O. Casals, E. Pellicier, J. Rodriguez, A. Romano-Rodriguez, J. R. Morante, S. Mathur, *Nanotechnology* **2007**, *18*, 424016; d) F. Yang, S. R. Forrest, *Adv. Mater.* **2006**, *18*, 2018.

[5] J. Sun, W. E. Buhro, *Angew. Chem.* **2008**, *120*, 3259; *Angew. Chem. Int. Ed.* **2008**, *47*, 3215.

[6] H. J. Fan, P. Werner, M. Zacharias, *Small* **2006**, *2*, 700.

[7] a) X. F. Duan, Y. Huang, Y. Cui, J. Wang, C. M. Lieber, *Nature* **2001**, *409*, 66; b) Y. Li, F. Qian, J. Xiang, C. M. Lieber, *Mater. Today* **2006**, *9*, 18; c) J. M. Bao, M. A. Zimmler, F. Capasso, *Nano Lett.* **2006**, *6*, 1719; d) X. F. Duan, Y. Huang, R. Argarawal, C. M. Lieber, *Nature* **2002**, *415–420*, 241; e) J. Kong, N. R. Franklin, C. W. Zhou, M. G. Chapline, S. Peng, K. Cho, H. J. Dai, *Science* **2000**, *287*, 622.

[8] a) Y. Wu, R. Fan, P. D. Yang, *Nano Lett.* **2002**, *2*, 83; b) K. Dick, K. Deppert, M. W. Larsson, T. Martensson, W. Seifert, L. R. Wallenberg, L. Samuelson, *Nat. Mater.* **2004**, *3*, 380; c) J. Xiang, A. Vidan, M. Tinkham, R. M. Westervelt, C. M. Lieber, *Nat. Nanotechnol.* **2006**, *1*, 208.

[9] a) W. I. Park, G. C. Yi, M. Kim, S. J. Pennycook, *Adv. Mater.* **2003**, *15*, 526; b) Y. J. Hsu, S. Y. Lu, *Chem. Commun.* **2004**, 2102.

[10] a) G. Z. Shen, C. Ye, D. Golbeg, J. Hu, Y. Bando, *Appl. Phys. Lett.* **2007**, *90*, 073115; b) J. Hu, Y. Bando, Z. Liu, D. Golberg, J. Zhan, *J. Am. Chem. Soc.* **2003**, *125*, 11307.

[11] R. Ostermann, D. Li, Y. D. Yin, J. T. McCann, Y. N. Xia, *Nano Lett.* **2006**, *6*, 1297.

[12] a) J. Y. Lao, J. G. Wen, Z. F. Ren, *Nano Lett.* **2002**, *2*, 1287; b) J. G. Wen, J. Y. Lao, D. Z. Wang, T. M. Kyaw, Y. L. Foo, Z. F. Ren, *Chem. Phys. Lett.* **2003**, *372*, 717.

[13] S. Y. Bae, H. W. Seo, H. C. Choi, J. Park, *J. Phys. Chem. B* **2004**, *108*, 12318.
[14] P. X. Gao, Z. L. Wang, *J. Phys. Chem. B* **2002**, *106*, 12563.
[15] H. Yan, R. He, J. Johnson, M. Law, R. J. Saykally, P. D. Yang, *J. Am. Chem. Soc.* **2003**, *125*, 4728.
[16] D. L. Wang, F. Qian, C. Yang, Z. H. Zhong, C. M. Lieber, *Nano Lett.* **2004**, *4*, 871.
[17] T. Y. Zhai, Z. J. Gu, H. Z. Zhong, Y. Dong, Y. Ma, H. B. Fu, Y. F. Li, J. N. Yao, *Cryst. Growth Des.* **2007**, *7*, 488.
[18] T. Y. Zhai, Z. J. Gu, Y. Dong, H. Z. Zhong, Y. Ma, H. B. Fu, Y. F. Li, J. N. Yao, *J. Phys. Chem. A* **2007**, *111*, 1030.
[19] C. Patel, S. Li, C. Wang, W. Zhang, Y. Wei, *Chem. Mater.* **2007**, *19*, 1231.
[20] Z. Y. Hou, C. X. Li, J. Yang, H. Z. Lian, P. P. Yang, R. T. Chai, Z. Y. Cheng, J. Lin, *J. Mater. Chem.* **2009**, *19*, 2737.
[21] M. Shang, W. Z. Wang, J. Ren, S. M. Sun, L. Wang, L. Zhang, *J. Mater. Chem.* **2009**, *19*, 6213.
[22] a) N. X. Wang, C. H. Sun, Y. Zhao, S. Y. Zhou, P. Chen, L. Jiang, *J. Mater. Chem.* **2008**, *18*, 3909; b) C. H. Sun, N. X. Wang, S. Y. Zhou, X. J. Hu, S. Y. Zhou, P. Chen, *Chem. Commun.* **2008**, 3293; c) C. H. Wang, C. L. Shao, X. T. Zhang, Y. C. Liu, *Inorg. Chem.* **2009**, *48*, 7261; d) M. Shang, W. Z. Wang, L. Zhang, S. M. Sun, L. Wang, L. Zhou, *J. Phys. Chem. C* **2009**, *113*, 14727.
[23] L. Vayssieres, *Adv. Mater.* **2003**, *15*, 464.
[24] K. Govender, D. S. Boyle, P. B. Kenway, P. O'Brien, *J. Mater. Chem.* **2004**, *14*, 2575.
[25] Q. Li, V. Kumar, Y. Li, H. Zhang, T. J. Marks, R. P. H. Chang, *Chem. Mater.* **2005**, *17*, 1001.
[26] A. N. Narkulov, D. K. Yunusov, V. A. Kim-Lin-Zu, *Z. Prik. Khim.* **1987**, *80*, 882.
[27] L. E. Greene, B. D. Yuhas, M. Law, D. Zitoun, P. D. Yang, *Inorg. Chem.* **2006**, *45*, 7535.
[28] L. E. Greene, M. Law, J. Goldberger, F. Kim, J. C. Johnson, Y. F. Zhang, R. J. Saykally, P. D. Yang, *Angew. Chem.* **2003**, *115*, 3139; *Angew. Chem. Int. Ed.* **2003**, *42*, 3031.
[29] a) H. Park, W. Choi, *J. Phys. Chem. B* **2003**, *107*, 3885; b) H. G. Kim, D. W. Hwang, J. S. Lee, *J. Am. Chem. Soc.* **2004**, *126*, 8912.
[30] a) M. R. Hoffmann, S. T. Martin, W. Choi, *Chem. Rev.* **1995**, *95*, 69; b) X. Wang, J. C. Yu, C. Ho, Y. Hou, X. Fu, *Langmuir* **2005**, *21*, 2552; c) L. Zhou, W. Z. Wang, H. L. Xu, S. M. Sun, M. Shang, *Chem. Eur. J.* **2009**, *15*, 1776; d) Y. Zhao, Y. Xie, X. Zhu, S. Yan, S. X. Wang, *Chem. Eur. J.* **2008**, *14*, 1601; e) M. Shang, W. Z. Wang, S. M. Sun, L. Zhou, L. Zhang, *J. Phys. Chem. C* **2008**, *112*, 10407.
[31] X. D. Zhu, S. R. Castleberry, M. A. Nanny, E. C. Butler, *Environ. Sci. Technol.* **2005**, *39*, 3784.
[32] W. Li, D. Li, Z. Chen, H. Huang, M. Sun, Y. He, X. Fu, *J. Phys. Chem. C* **2008**, *112*, 14943.
[33] F. Zhang, S. S. Wong, *Chem. Mater.* **2009**, *21*, 4541.
[34] J. Wu, F. Duan, Y. Zheng, Y. Xie, *J. Phys. Chem. C* **2007**, *111*, 12866.
[35] J. Wang, M. S. Gudiksen, X. Duan, Y. Cui, C. M. Lieber, *Science* **2001**, *293*, 1455.
[36] H. X. Li, Z. F. Bian, J. Zhu, D. Q. Zhang, G. S. Li, Y. N. Huo, H. Li, Y. F. Lu, *J. Am. Chem. Soc.* **2007**, *129*, 8406.

Received: March 12, 2010
Published online: August 16, 2010

